AD-A174 892 THERMAL TRANSPORT PROPERTIES IN THE PRIMARY GAS-PHASE 1/1
COMBUSTION ZONE OF (U) ARMY BALLISTIC RESEARCH LAB
ABERDEEN PROVING GROUND MD M S MILLER ET AL SEP 86
UNCLASSIFIED BRL-MR-3545 F/G 21/2 NL

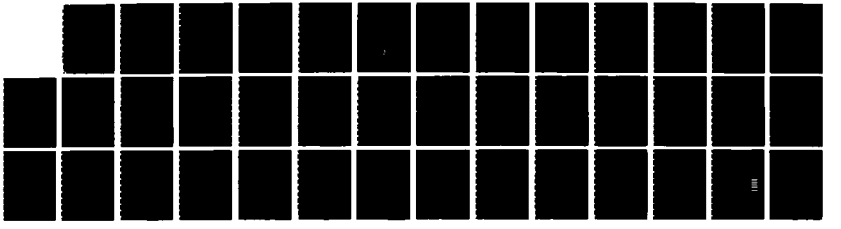

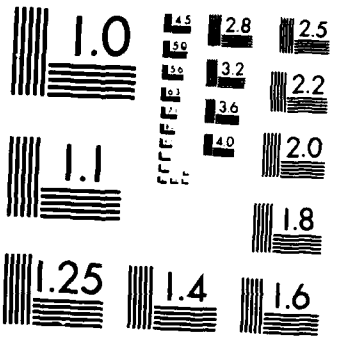

US ARMY
MATERIEL
COMMAND

MEMORANDUM REPORT BRL-MR-3545

THERMAL TRANSPORT PROPERTIES IN THE PRIMARY GAS-PHASE COMBUSTION ZONE OF DOUBLE-BASE PROPELLANT: A SENSITIVITY STUDY

Martin S. Miller
Anthony J. Kotlar

September 1986

US ARMY BALLISTIC RESEARCH LABORATORY
ABERDEEN PROVING GROUND, MARYLAND

Destroy this report when it is no longer needed.
Do not return it to the originator.

Additional copies of this report may be obtained from the National Technical Information Service, U. S. Department of Commerce, Springfield, Virginia 22161.

The findings in this report are not to be construed as an official Department of the Army position, unless so designated by other authorized documents.

The use of trade names or manufacturers' names in this report does not constitute indorsement of any commercial product.

UNCLASSIFIED
SECURITY CLASSIFICATION OF THIS PAGE

AD-A174 872

REPORT DOCUMENTATION PAGE

Form Approved
OMB No 0704-0188
Exp Date Jun 30, 1986

1a REPORT SECURITY CLASSIFICATION Unclassified	1b RESTRICTIVE MARKINGS
2a SECURITY CLASSIFICATION AUTHORITY	3 DISTRIBUTION / AVAILABILITY OF REPORT Approved for Public Release; Distribution Unlimited.
2b DECLASSIFICATION / DOWNGRADING SCHEDULE	
4 PERFORMING ORGANIZATION REPORT NUMBER(S) Memorandum Report BRL-MR-3545	5 MONITORING ORGANIZATION REPORT NUMBER(S)
6a NAME OF PERFORMING ORGANIZATION US Army Ballistic Research Laboratory 6b OFFICE SYMBOL (If applicable) SLCBR-IB	7a NAME OF MONITORING ORGANIZATION
6c ADDRESS (City, State, and ZIP Code) Aberdeen Proving Ground, MD 21005-5066	7b ADDRESS (City, State, and ZIP Code)
8a NAME OF FUNDING / SPONSORING ORGANIZATION 8b OFFICE SYMBOL (If applicable)	9 PROCUREMENT INSTRUMENT IDENTIFICATION NUMBER
8c ADDRESS (City, State, and ZIP Code)	10 SOURCE OF FUNDING NUMBERS PROGRAM ELEMENT NO: 61102A; PROJECT NO: AH43; TASK NO:; WORK UNIT ACCESSION NO:

11 TITLE (Include Security Classification)
THERMAL TRANSPORT PROPERTIES IN THE PRIMARY GAS-PHASE COMBUSTION ZONE OF DOUBLE-BASE PROPELLANT: A SENSITIVITY STUDY

12 PERSONAL AUTHOR(S)
Martin S. Miller and Anthony J. Kotlar

13a TYPE OF REPORT	13b TIME COVERED	14 DATE OF REPORT (Year, Month, Day)	15 PAGE COUNT
Final	FROM Apr85 TO Jul86	September 1986	37

16 SUPPLEMENTARY NOTATION

17 COSATI CODES			18 SUBJECT TERMS (Continue on reverse if necessary and identify by block number)
FIELD	GROUP	SUB-GROUP	Double-Base Propellant, Fizz Zone Gases, Thermal Conductivity, Specific Heat, Burning Rate Model, Sensitivity Study
21	02		
21	09.2		

19 ABSTRACT (Continue on reverse if necessary and identify by block number)

Economies in both time and expense can be achieved in the design of propelling charges for guns by the use of mathematical models of the interior ballistic cycle. Continued development of such models is impeded by the need to describe the kinetics controlling the propellant heat release in a more realistic way. Work toward this goal has thus far shown that the use of overall reactions to describe flames with complex kinetics can preserve the key thermal features of the flame such as the temperature and heat release profiles and flame speed. A method has also been developed for determining the kinetic parameters of this overall reaction from a temperature profile measured in the combustion wave. The kinetics extraction technique, however, requires knowledge of the thermal conductivity and specific heat of the gas mixture through the zone of heat release. Uncertainties in these transport properties stem from uncertainties in the molecular composition in the combustion zones of propellants. This study assesses the probable error in best estimates of the transport parameters and determines how this error propagates through the kinetics

20 DISTRIBUTION / AVAILABILITY OF ABSTRACT	21 ABSTRACT SECURITY CLASSIFICATION
☐ UNCLASSIFIED/UNLIMITED ☒ SAME AS RPT ☐ DTIC USERS	Unclassified
22a NAME OF RESPONSIBLE INDIVIDUAL DR. MARTIN S. MILLER	22b TELEPHONE (Include Area Code) 301-278-6156 / 22c OFFICE SYMBOL SLCBR-IB-I

DD FORM 1473, 84 MAR

83 APR edition may be used until exhausted
All other editions are obsolete

SECURITY CLASSIFICATION OF THIS PAGE
UNCLASSIFIED

19. Abstract:

extraction technique and into a calculation of the burning rate based on the derived kinetics. The resultant errors turn out to be modest, and a major effort to measure the molecular composition for this purpose does not appear warranted at present.

TABLE OF CONTENTS

LIST OF FIGURES

LIST OF TABLES

I. INTRODUCTION

The chemical reaction steps involved in the combustion of solid propellant are poorly understood. For this reason the mathematical modeling of propellant combustion has most often relied on overall reaction descriptions of the detailed kinetics in each macroscopic combustion zone. The success with which these overall reactions can mimic the effects of complex kinetics has been demonstrated previously.[1-3] A technique for determining the overall kinetic parameters from measured temperature profiles has also been developed.[4] This technique utilizes the energy conservation equation to compute the volumetric heat release profile, from which the kinetics are derived in various ways. Apart from the spatial derivatives of the temperature, the energy equation also involves the thermal conductivity and specific heat of the local gas mixture. In the development of the kinetics extraction technique it was necessarily assumed that these values were known. The present study was undertaken to assess the extent to which current uncertainties in these transport parameters jeopardizes burning rate predictions based on this kinetics extraction technique.

The need for this assessment arose during a study of the feasibility of molecular beam sampling of the stable intermediate chemical species present during solid propellant combustion. Molecular beam sampling of radicals had been attempted previously but suffered from low signal strengths. Renewed interest in the experiment was generated by the desire for major species profiles in combusting nitramines as well as by the potential use in estimating the transport properties of fizz zone gases for the application described above. It was felt that such an assessment would not only help determine if the molecular beam experiment was warranted but might also produce best estimates of these transport parameters for interim use.

We begin with a discussion of experiments in which gas compositions were determined at the beginning and end of the fizz zone of burning double base propellants. The thermal conductivity and specific heat are then calculated for these mixtures and models for the temperature dependence of the properties are constructed. Concentrations of key species are then varied within limits thought to reflect maximum probable experimental uncertainties, and the mixture properties recomputed for these extremes. These calculations form the basis for making best a priori estimates of the actual mixture properties and the maximum probable errors associated with these estimates. The extent to which these errors map into the derived kinetics parameters and ultimately into burning rate predictions is then determined. (In this report the term "burning rate" will refer to the surface regression rate in either its linear form or mass flux form.)

II. MOLECULAR COMPOSITION OF THE PRIMARY FLAME ZONE

Lengelle, et al.,[5] have summarized the current state of knowledge with regard to the molecular composition of the gases beyond the burning surface of solid double-base propellant. Heat release in the gas phase occurs in two stages which here will be termed the primary and secondary flame zones. The primary flame is also known as the fizz zone and is non-luminous in contrast to the secondary flame. Below about 1 MPa, the propellant burns without a secondary flame and the full heat of explosion is consequently not achieved.

At its onset the secondary flame stabilizes at a distance on the order of a centimeter from the surface. As the pressure is increased, the secondary flame moves closer to the surface until at 5-10 MPa it appears to be in contact with the surface. At these pressures the combustion zones are too compressed to know if the two-stage character remains or if they coalesce into a single zone. The primary zone appears to consist of reactions of NO_2 with aldehydes, and the secondary flame is dominated by NO reacting with CO and H_2. At pressures where the two stage character pertains, the preponderance of evidence suggests that the burning rate is controlled by the primary flame alone. Accordingly, the focus in this study is on the gases of the primary flame.

An experiment which simulates a measurement of the gases emerging from the burning surface has been described by Lengelle, et al.[5,6] Under vacuum, propellant is subjected to either a heated, perforated plate or radiant heating such that a surface regression rate of about 1 mm/s is achieved. These conditions allow a residence time in the condensed phase similar to that occuring during combustion but prevent the primary gas flame from developing. The gases issuing from the surface are sampled through a probe, then ionized and analyzed by mass spectrometry. The molecular compositions determined from this experiment are given in Table 1.

Table 1. Surface Gas Composition (600 K)

	CH_2O	$(CHO)_2$	CO	CO_2	NO_2	NO	H_2O	H_2
λ_i X 10^4	1.75_n	2.05^*_e	1.06_t	0.963_t	0.999_t	1.10_t	1.11_t	6.95_t
c_{pi}	0.383_n	$0.780^{\#}_e$	0.260_n	0.257_n	0.238_n	0.249_n	0.481_n	3.48_n
X_i (EXP.)	0.23	0.11	0.13	0.06	0.28	0.11	0.06	0.02
m_i (EXP.)	0.19	0.18	0.10	0.07	0.34	0.09	0.03	0.001
X_i (HIGH)	0.46	0.22	0.06	0.03	0.12	0.05	0.03	0.04
m_i (HIGH)	0.37	0.34	0.05	0.04	0.15	0.04	0.01	0.002
X_i (LOW)	0.12	0.06	0.16	0.08	0.35	0.14	0.08	0.01
m_i (LOW)	0.10	0.10	0.12	0.10	0.44	0.11	0.04	0.0005

Notes:

λ in cal/cm-s-K c_p in cal/g-K

t - Touloukian, et al.[12]

n - NASA-Lewis code[13]

e - estimate based on methane (see text)

* - a value of 1.0×10^{-4} was used for the LOW calculation

- a value of 0.30 was used for the LOW calculation

EXP. - experimental values,[5] X_i are mole fractions, m_i are mass fractions

Experiments under similar conditions have been conducted by other investigators as well. Dauerman and Tajima[7-9] applied mass spectrometry with a cone-type sampling port to the radiative pyrolysis of double-base propellant at pressures up to 100 torr. Although NO_2 was observed, they argued that NO_3 was the primary oxidizer formed in the breakup of the $-CONO_2$ groups. Later work by Farber and Srivastava[10] using mass spectrometric analysis of gases produced in heated effusion cells supported the direct production of NO_2 under vacuum pyrolysis conditions.

Lengelle, et al.,[5] have also extracted samples of the gases at the end of the primary flame zone through small probes and analyzed them with mass spectrometry and gas chromatography. The composition obtained for propellant burning at 9 atm is given in Table 2. This breakdown agrees substantially with similar measurements made previously by Heller and Gordon.[11]

Table 2. Dark Zone Gas Composition (1600 K)

	N_2	NO	CO	CO_2	CH_4	C_2H_4	H_2O	H_2
$\lambda_i \times 10^{-4}$	2.13_t	2.42_n	2.27_n	2.46_t	6.69_n	4.80_n	5.18_n	15.6_n
c_{pi}	0.300_n	0.287_n	0.303_n	0.320_n	1.32_j	0.950_n	0.636_n	3.88_n
X_i (EXP.)	0.02	0.21	0.38	0.09	0.03	0.01	0.20	0.08
m_i (EXP.)	0.02	0.25	0.42	0.15	0.02	0.01	0.32	0.006
X_i (HIGH)	0.01	0.11	0.20	0.05	0.05	0.02	0.04	0.16
m_i (HIGH)	0.01	0.16	0.28	0.11	0.04	0.03	0.35	0.01
X_i (LOW)	0.02	0.26	0.47	0.10	0.01	0.005	0.10	0.04
m_i (LOW)	0.02	0.28	0.47	0.16	0.01	0.005	0.06	0.004

Notes:

λ in cal/cm-s-K c_p in cal/g-K

t - Touloukian, et al.[12]

n - NASA-Lewis code[13]

j - JANAF tables[17]

EXP. - experimental values,[5] X_i are mole fractions, m_i are mass fractions

III. THERMAL CONDUCTIVITY FOR INDIVIDUAL SPECIES AND MIXTURES

Values for the thermal conductivity of individual species in Tables 1 and 2 are, for the most part, obtained from the data compilation by Touloukian, et al.,[12] or the NASA-Lewis code.[13] In general the Touloukian and NASA-Lewis values agreed closely with those computed by the modified Eucken correlation[14] in which the viscosity was calculated using the Lennard-Jones potential.[14] In

the case of glyoxal, neither conductivity data nor L-J parameters could be found, so the values for methane[12] were used as a reasonable upper limit since no organic molecule in the Touloukian compilation has a higher conductivity.

Thermal conductivities for the multicomponent mixtures are obtained using a combination of the linear and reciprocal mixing rules.[12,15]

$$\lambda_{mix} = 0.5\ [\Sigma_i\ X_i\lambda_i + \{\Sigma_i\ (X_i/\lambda_i)\}^{-1}] \quad ,$$

where X_i is the mole fraction of the species i and λ_i is the thermal conductivity of the species i. This empirical equation has been found[12] to minimize error in the mixture conductivity since the linear rule leads to overestimates and the reciprocal rule leads to underestimates.

The pressure dependence of the thermal conductivity was also considered. The estimation procedure of Stiel and Thodos[14,16] was used to compute the variation of thermal conductivity with pressure for the individual species; then, the mixture value was obtained by the above empirical rule. At 9 atm the mixture conductivity was increased over the 1 atm value by less than 1%. At 50 atm the increase was less than 5%. Thus only the 1 atm values are given in Tables 1 and 2.

IV. SENSITIVITY OF MIXTURE THERMAL CONDUCTIVITIES AND SPECIFIC HEATS TO VARIATIONS IN COMPOSITION

In an effort to determine how experimental uncertainties in the above molecular compositions might affect the mixture thermal conductivity and specific heat, we have arbitrarily doubled (and halved) the mole fractions of the species with the highest values for the thermal conductivity. Barring gross systematic errors in the experiments, this strategy should lead to an estimate of the maximum probable error in the mixture parameters. In Tables 1 and 2 the underscored mole fractions were varied as just described and the remaining mole fractions recomputed in their same relative proportions. The mixture specific heat is calculated as the linear sum of the mass-fraction-weighted individual specific heats. The results are summarized in Table 3. Also indicated in the table are the percent errors in the experimental values should the extreme values be correct. It is clear that one could choose average values for which the maximum probable error would be less than 25% for the thermal conductivity and less than 30% for the specific heat.

The variation scheme adopted is obviously not unique and is not even completely self-consistent, since atomic mass fractions are not conserved. However, because of the similarity of transport parameter values among species not underlined in Tables 1 and 2, attending to these details would produce only minor corrections to our analysis. Also, use of the methane value for thermal conductivity in the case of glyoxal, while sensible in obtaining an upper limit for the transport parameters, is inappropriate for obtaining the lower limit. Again, however, in the lower limit case, the mole fraction of glyoxal is too small to influence the mixture value so that our object is not jeopardized by this apparently poor assumption. If, in fact, these transport parameter variations did lead to large influences on the burning rate predictions, then more care in their construction would be in order. As will be seen, no such result is obtained.

Table 3. Mixture Properties

Property	Experimental	High	Low
λ (cal/cm-s-K) @ 600 K	1.34E-4	1.68E-4 (20%)*	1.14E-4 (18%)
c_p (cal/g-K) @ 600 K	0.378	0.488 (23%)	0.278 (36%)
λ (cal/cm-s-K) @ 1600 K	3.51E-4	4.87E-4 (28%)	2.90E-4 (21%)
c_p (cal/g-K) @ 1600 K	0.395	0.550 (28%)	0.348 (14%)

* % error in the experimental value if this were the true value.

V. EFFECT OF UNCERTAINTY IN λ AND c_p ON HEAT RELEASE PROFILES, OVERALL KINETICS, BURNING RATE, AND TEMPERATURE SENSITIVITY

In order to probe the effects of the uncertainties in transport properties on the derived kinetics, we have assembled five transport models from the high and low values given in Table 3. Each model assumes a temperature dependence for both the thermal conductivity and specific heat of the form

$$f = aT^b \quad ,$$

where f is the transport property being considered and T is the temperature in Kelvins. The constants a and b for the five cases are chosen so as to give: (1) the maximum values for thermal conductivity over the range 600-1600 K (labeled MAXV in the figures), (2) the maximum slope with respect to temperature (MAXS), (3) the minimum values (MINV), (4) minimum slope (MINS), and (5) the best estimate (BESTE) of the values over the interval. The best estimate at each temperature is chosen so as to equalize the percent error between the best estimate and extreme values in Table 3. This criterion leads to the defining expression (at each end of the temperature interval)

$$f_{be} = 2\, f_H\, f_L/(f_H + f_L) \quad , \qquad (1)$$

where f_L and f_H are the low and high values of the transport parameter f from Table 3. The temperature dependence of the best estimate model is then constructed according to the power law function above. The values of a and b for all five cases are given in Table 4, and the five models for $\lambda(T)$ and $c_p(T)$ are plotted in Figures 1 and 2, respectively, to illustrate how they span the range of possibilities. In the following analysis we shall adopt the point of view that the best estimate model is the least biased guess to use in the analysis of fizz zone temperature profiles. We then suppose that, due to errors in the experimental compositions, the actual values of λ and c_p might be given by one of the other four models. The consequences of these errors can then be assessed in relation to calculations based on the corresponding transport model.

Table 4. Defining Parameters for $\lambda(T)$ and $c_p(T)$ Models

Parameter	Min. Slope	Min. Value	Best Est.	Max. Slope	Max. Value
a (for λ)	4.7756E-6	2.5840E-7	2.2131E-7	8.7902E-9	1.6245E-7
b (for λ)	0.55659	0.95193	1.0037	1.4804	1.0851
a (for c_p)	4.4270	6.4258E-2	0.10583	3.2469E-3	0.22369
b (for c_p)	-0.34472	0.22897	0.18876	0.69563	0.12194

Note: λ in cal/cm-s-K, c_p in cal/g-K

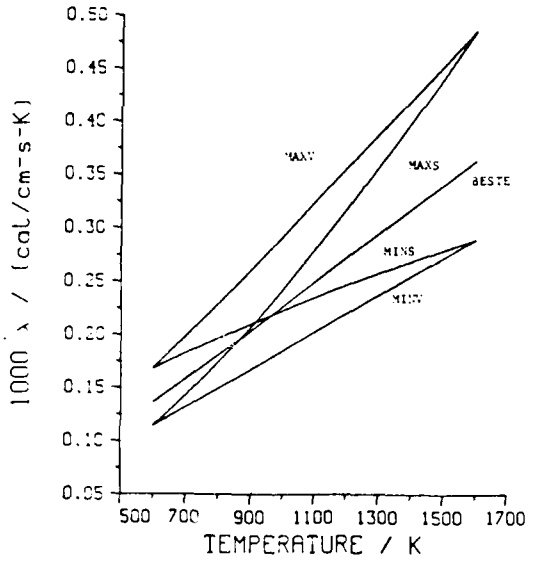

Figure 1. Models of Mixture Thermal Conductivity in the Primary Combustion Zone Based on Maximum Probable Uncertainties in Molecular Compositions

The technique for deriving overall kinetics from a combustion wave temperature profile is described in detail in Ref. 4. Essentially, it depends on the energy conservation equation simplified by assuming that the specific heats of all chemical species are equal and that thermal diffusion is negligible. In that case

$$(d/dx)[\lambda(dT/dx)] - Mc_p(dT/dx) + q(x) = 0 \quad , \qquad (2)$$

where q(x) is the volumetric rate of heat release due to reactions (also referred to here as the heat release profile). Equation 2 is valid for

temperature dependences in both λ and c_p (though Ref. 4 assumed λ and c_p to be constant). First, the temperature profile is least squares fitted by a suitable but arbitrary analytic function (see the appendix). The temperature derivatives in Eq. 2 can then be obtained analytically and together with values for λ and c_p one can calculate the heat release profile, q(x). The heat release profile is related to the kinetics by[4]

$$q = Q_g (\rho m_B)^{\nu} A_g \exp(-E_g/RT) \quad ,$$

where Q_g (cal/g) is the primary flame zone heat release, ρ is the local mass density, m_B is the mass fraction of our single hypothetical reactant, ν is the order of the overall reaction with respect to that reactant's concentration, A_g is the Arrhenius preexponential factor, and E_g is the activation energy. The overall kinetics can be derived from the heat release profile as described in Ref. 4. (The "single point method" is used exclusively here.)

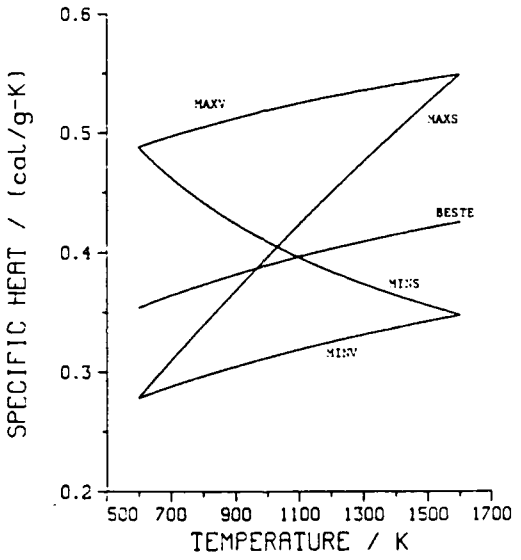

Figure 2. Models of Mixture Specific Heat in the Primary Combustion Zone Based on Maximum Probable Uncertainties in Molecular Compositions

In this study the procedure was applied to the experimental temperature profile published by Zenin[18] for a double base propellant burning at 1.0 MPa and 25°C. These data were chosen because the temperature profile, surface temperature, and burning rate were all measured in the same experiment. In publishing his temperature profiles Zenin used his measured value of the surface temperature to locate the origin of coordinates at the surface. Because of small errors in digitizing the temperature profiles, the value of surface temperature given by the analytic fit evaluated at the surface is 605 K rather than his reported value of about 570 K. To avoid inconsistencies we simply take the experimental surface temperature value in this study to be 605 K.

It should be noted that the objective of this approach is to obtain an accurate and convenient description of the thermal structure of the fizz zone and not a detailed understanding of the chemical kinetics. Therefore the method should ultimately be judged by the fidelity with which the temperature and heat release profiles, computed by means of the derived kinetics in a single-reaction flame code, can mimic the original (i.e., measured T(x) and derived q(x)) profiles. In Ref. 4 it was shown that if a given temperature profile was caused by a single irreversible reaction, and if λ and c_p for the system are known, then the kinetic parameters can be recovered by the above procedure with good accuracy. It was also demonstrated that overall kinetics derived from an actual fizz zone temperature profile, when used as input to a flame code, did indeed enable an accurate reconstruction of both the temperature and heat release profiles, again assuming knowledge of λ and c_p for the gases.

Uncertainties in λ and c_p give rise to uncertainties in the heat release profile from which the kinetics are derived. Since the shapes of the heat release profiles based on the different transport models are similar, differences can be summarized by the magnitudes and positions of the peak in q(x), which is computed from the fitted temperature profile using Eq. 2. Peak values and positions for all the transport models are shown in Figure 3. That figure indicates that use of the best estimate model results in the errors of the peak magnitude of probably no more than 25% but errors in the peak position of as much as a factor of 2. The possible significance of these errors will be discussed presently.

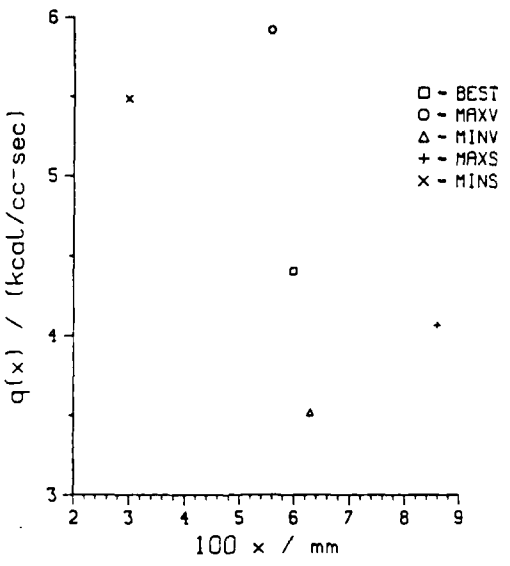

Figure 3. Magnitudes and Positions of Peaks in the Heat Release Profiles Determined from Zenin's Fizz Zone Temperature Profile (at 10 atm) and the Various Thermal Transport Models

Table 5 shows how the different transport models affect the determination of the overall kinetics parameters. Uncertainties of up to 25% arise in the activation energy; however, the significance of this variation is best judged

in relation to its effects on model burning rate calculations which are discussed next.

Table 5. Model Parameters Determined Directly from the Analytic Fit to the Temperature Profile

Parameter	Min. Slope	Min. Value	Best Est.	Max. Slope	Max. Value
ϕ (cal/cm^2-s)*	6.17 (-19%)	4.20 (+19%)	5.01	4.22 (+19%)	6.20 (-19%)
Q_g(cal/g)	353. (-7%)	264. (+25%)	329.	333. (-1%)	437. (-25%)
Q_s(cal/g)	171. (-45%)	51. (+84%)	94.	52. (+81%)	172. (-45%)
E_g(kcal/mole)	2.55 (+24%)	3.32 (-5%)	3.17	4.12 (-23%)	2.95 (+7%)
ν	0.71	0.72	0.70	0.73	0.67
A_g(cgs units)	4.15E3	5.82E3	4.79E3	8.78E3	3.72E3

Notes: Based on the experimental values, M=0.32 g/cm^2-s, T_s=605 K, and T_0=298 K.
Percent errors are computed assuming that the extreme transport models may be correct.
*$\phi \equiv \lambda \, (dT/dx)_s$ is the heat feedback flux from the gas to the burning surface.

In order to do a calculation of the burning rate, a number of parameters besides the gas phase kinetics are required. We now discuss briefly how one might obtain these values. Physical and mathematical details of the combustion idealization employed here are discussed in Refs. 19-21. Given a temperature profile in the gas phase, the mass burning rate M, the surface temperature T_s, all determined experimentally, and models for λ and c_p, the effective gas phase kinetics can be determined as described above. In addition, the gas phase heat release can be deduced from (see eqs. 15 and 23 of Ref. 19, here generalized for a temperature dependent specific heat)

$$Q_g = \int_{T_S}^{T_f} c_p \, dT + (\lambda/M) \, (dT/dx)_s \quad , \tag{3}$$

where λ is evaluated at T_s and we have set the nascent gas-phase reactant mass fraction (m_B^{-0} in Ref. 19) to 1 in the absence of more detailed information. T_f is the temperature at the end of the fizz zone and is here taken as the fitted value at the last digitized point. The condensed phase heat release may be obtained from the energy flux continuity condition (Eq. 18 of Ref. 19) at the gas/solid interface:

$$Q_s = c_p \, T_s - c_s \, T_0 - (\lambda/M) \, (dT/dx)_s \quad , \tag{4}$$

where T_0 is the ambient temperature of the propellant strand at the start of the temperature profile experiment and c_p is evaluated at T_s. The condensed phase specific heat, c_s, could be measured using standard thermal analysis methods. Here we assume a constant value of 0.35 cal/g-K. Like the gas phase kinetics and Q_g, Q_s will be sensitive to the transport models as shown in Table 5.

The parameters for the pyrolysis law, which is assumed to govern the surface regression, may be obtained from measurements of the burning rate and surface temperature at a number of different pressures and initial temperatures. This was done in Ref. 20 (NC3 data set) for data reported by Zenin. Here we make use of the activation energy so determined and compute a preexponential factor M_0, consistent with the fitted surface temperature and measured burning rate for the temperature profile used in this work. The pyrolysis law in terms of the mass regression rate is

$$M = M_0 \exp(-E_s/RT_s) \quad . \tag{5}$$

With all of the model parameters now semi-empirically determined, one may solve the conservation equations numerically (as was done in Ref. 21) for the burning rate, temperature profile, and heat release profile. These calculated quantities may then be compared with the "experimental" ones. (Quotes are used because the original heat release profile requires estimates of the transport parameters and thus is really a derived result.) Results of this "complete solution" are shown in Figures 4-8 and in Table 6 for each of the transport models (all figures using the same scale for easy comparison). In the figures the discrete points are the digitized values of Zenin's experimentally determined temperature profile. The solid curve through these points is the analytic temperature function derived by a least squares fit to the discrete points (see Appendix A). These two curves are the same for all five transport models. The solid curve with the maximum is the heat release profile derived from the analytic temperature profile with the indicated transport models. (The magnitude and position of the peak of this profile are the values shown in Figure 3.) The dashed temperature profile is the solution of the energy equation using the derived kinetics and Eq. 4 as the solid-gas boundary condition. The dashed heat release profile is constructed from the overall kinetics and the dashed temperature profile. For each transport case it is seen that the calculated profiles match the "experimental" profiles quite closely over the bulk of the reactive heat release. The slow rise of the experimental temperature after the shoulder is characteristic of relatively slow recombination reactions[1] and would require a separate effective reaction to model. Such an effort is hardly appropriate in view of the small amount of energy involved.

The first conclusion to be drawn from an examination of Figures 4-8 and Tables 5 and 6 is that the ability of the analysis method to mimic the experimental temperature profile, match the experimental burning rate, and give a self-consistent rendering of the heat release profile is remarkably good for each model of the transport parameters. To some extent the high degree of numerical consistency is due to the self-compensating effect of using the same transport model to solve the conservation equations as was used to derive the kinetics. Since both Q_s and Q_g were obtained using the experimental values of M, T_s, and T_0, these conditions constitute something of a "calibration point," i.e., if the overall reaction description were

perfectly able to mimic the actual thermal structure, one would expect to back calculate the experimental value of the burning rate at the calibration point. Thus the very small errors in the back calculated burning rates provide an indication of the basic compatability of the single overall reaction idealization with the actual fizz zone reaction phenomena.

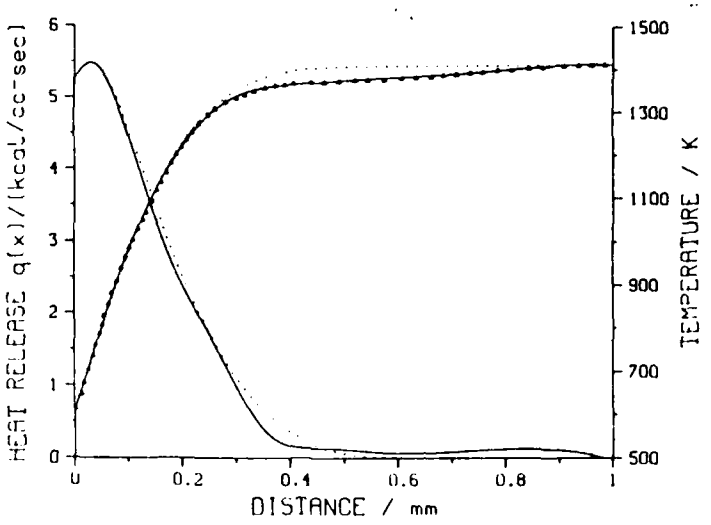

Figure 4. Calculated (Dashed Lines) Temperature and Heat Release Profiles Based on Effective Kinetics Derived from the Heat Release Profile (Solid Line) Deduced from the Analytic Fit (Solid Line) to Zenin's Temperature Profile Data (Points) and the Minimum Slope (MINS) Transport Model

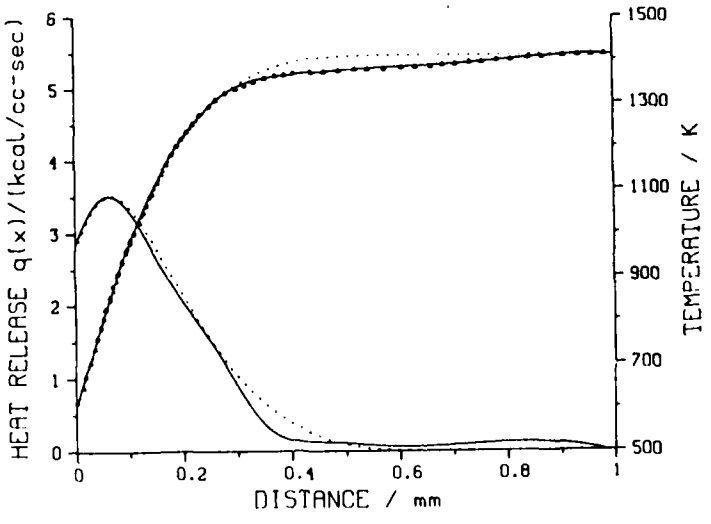

Figure 5. Calculated (Dashed Lines) Temperature and Heat Release Profiles Based on Effective Kinetics Derived from the Heat Release Profile (Solid Line) Deduced from the Analytic Fit (Solid Line) to Zenin's Temperature Profile Data (Points) and the Minimum Value (MINV) Transport Model

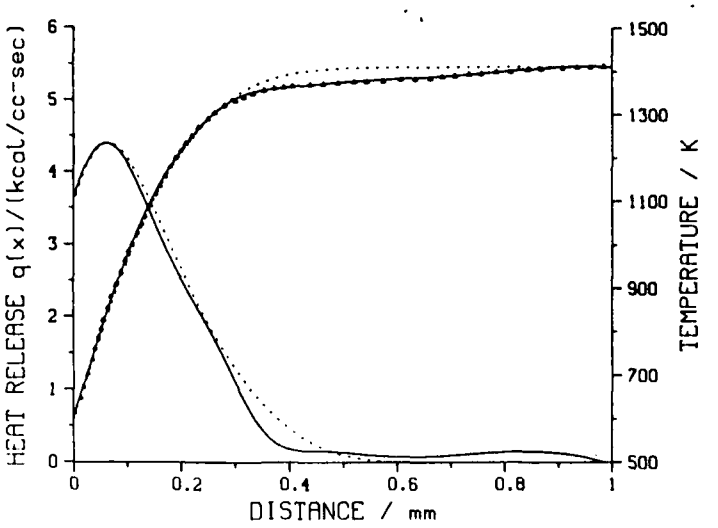

Figure 6. Calculated (Dashed Lines) Temperature and Heat Release Profiles Based on Effective Kinetics Derived from the Heat Release Profile (Solid Line) Deduced from the Analytic Fit (Solid Line) to Zenin's Temperature Profile Data (Points) and the Best Estimate (BESTE) Transport Model

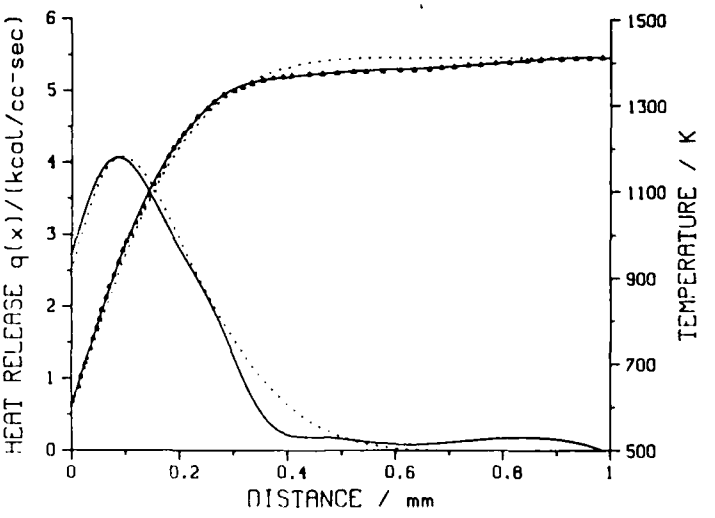

Figure 7. Calculated (Dashed Lines) Temperature and Heat Release Profiles Based on Effective Kinetics Derived from the Heat Release Profile (Solid Line) Deduced from the Analytic Fit (Solid Line) to Zenin's Temperature Profile Data (Points) and the Maximum Slope (MAXS) Transport Model

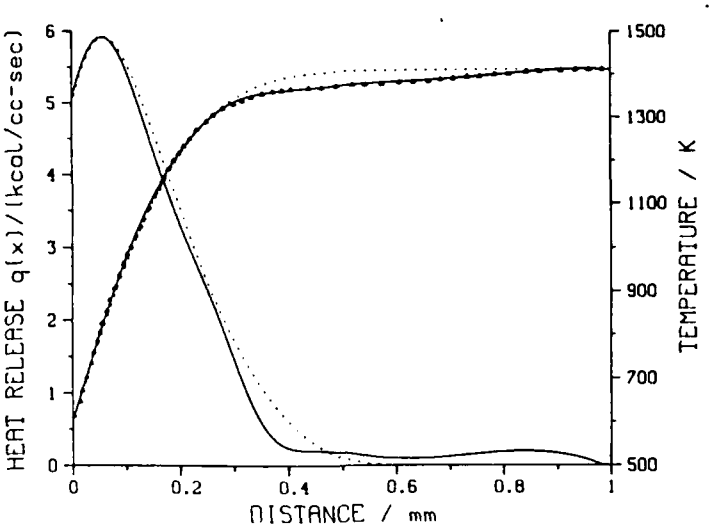

Figure 8. Calculated (Dashed Lines) Temperature and Heat Release Profiles Based on Effective Kinetics Derived from the Heat Release Profile (Solid Line) Deduced from the Analytic Fit (Solid Line) to Zenin's Temperature Profile Data (Points) and the Maximum Value (MAXV) Transport Model

Secondly, it is apparent that our uncertainty in the transport parameters does not affect a model calculation of the burn rate significantly, i.e., by no more than two percent. The heat flux, $\phi=\lambda(dT/dx)_s$, to the burning surface is somewhat more sensitive, in the range of 20-30%. This latter observation may be significant for use of the model under transient combustion conditions. On the whole, however, at least for the steady-state combustion case studied, the effectiveness of the analysis is not particularly sensitive to probable uncertainties in λ and c_p.

These results constitute an important finding; however, they only satisfy a necessary condition for the ultimate utility of the strategy. A more stringent test is afforded by comparing burning rate calculations at ambient temperatures other than the "calibration point" of 298 K. Except for certain catalyzed double-base propellants, it is generally observed that burning rates increase with increasing ambient temperature. The rate of increase is governed by a complex interaction of effects involving both gas-phase kinetics, pyrolysis law, and reaction heats. One thus expects that the different model parameter sets given in Table 5 will lead to different ambient temperature dependencies in the burning rate. For these calculations, the derived kinetics, with Eq. 4 as the boundary condition, are again used to calculate the thermal structure and mass burning rate. In this case, however, the value of Q_s, assumed to be constant, is fixed at the appropriate value computed at the calibration temperature (see Table 5), but now different ambient temperatures, T_0, are chosen, and a corresponding value for m is calculated. Figure 9 illustrates the different ambient temperature dependencies for the transport models that produce the largest variation from the best estimate case. As summarized in Table 6, the effect of uncertainty in transport parameters on the burning rate is magnified but still 7% or less over the practical temperature range (250-350 K).

Table 6. Complete Solution Results for Derived Kinetics

Paramenter @ T_0	Min. Slope	Min. Value	Best Est.	Max. Slope	Max. Value
ϕ (cal/cm^2-s) @ 298 K	6.04 (-22%)	3.92 (+20%)	4.63	3.62 (+30%)	5.81 (-20%)
M (g/cm^2-s) @ 298K	0.3173 (-1.1%)	0.3136 (+0.1%)	0.3139	0.3092 (+1.5%)	0.3144 (-0.2%)
M (g/cm^2-s) @ 250K	0.2466 (-1.1%)	0.2320 (+5.2%)	0.2440	0.2375 (+2.7%)	0.2571 (-5.1%)
M (g/cm^2-s) @ 350K	0.4427 (-3.7%)	0.4570 (-6.7%)	0.4264	0.4185 (+1.9%)	0.3986 (+7.0%)
M (g/cm^2-s) @ 400K	0.6444 (-10%)	0.6696 (-13%)	0.5828	0.5597 (+4.1%)	0.5074 (+15%)

Note: Percent errors are computed assuming that the extreme transport models may be correct.

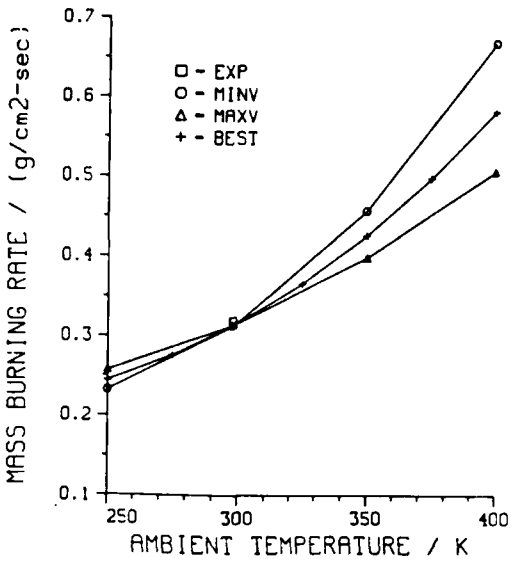

Figure 9. Mass Burning Rates Computed as a Function of Ambient Temperature Using Effective Kinetics Derived from Zenin's 10 atm Data at 300 K

VI. TRANSPORT PROPERTIES OF THE SECONDARY FLAME ZONE: AN ASIDE

In this paper and others to date[4 19 20 21 22] we have been concerned with describing the primary flame zone reactions because the preponderance of evidence suggests that the secondary flame zone does not affect the burning rate at low pressure. The secondary flame reactions are of importance, however, to interior ballistics since they release about half of the total chemical heat. Consequently, they exert a strong influence on flamespreading and ignition times. The method developed for deriving the effective kinetics for the primary flame is equally applicable to the secondary flame, given a temperature profile through that region. The transport parameters for that combustion zone are therefore also of interest. The purpose of the section is to establish best estimates for these transport parameters for eventual use in determining the effective kinetics of the secondary flame.

Fifer and Cohen[23] have reported calculations of the thermal conductivity and specific heat of final gas phase products from combustion of black powder, HMX, M30 propellant, and M9 propellant. The focus of that work was on the effects of shifts in the equilibrium species concentrations due to drops in temperature in boundary layers. Results are presented in terms of the "frozen" and "reactive" contributions to the effective transport parameters. The frozen component is based on mixing rules applied to the properties of the species concentrations at equilibrium at some given temperature and is equivalent to the mixture properties calculated in this paper. The reactive component arises when one considers steady-state heat flow in reactive systems in the absence of convection in the direction of the temperature gradient. In terms of the overall reaction picture, one has a single reactant of mass fraction m, which changes according to the species continuity equation (Eqs. 3 and 5, Ref. 19),

$$(d/dx)[D\rho(dm/dx)] + q(x)/Q_g = 0 \quad . \tag{6}$$

Solving for q(x) and substituting into Eq. 2 (with M=0), one gets

$$(d/dx)[(\lambda + Q_g D\rho(dm/dT))(dT/dx)] = 0 \quad . \tag{7}$$

Thus one recovers the simple heat conduction equation where the reacting gas behaves like a pure gas of equivalent thermal conductivity λ_{eff} defined by

$$\lambda_{eff} = \lambda + Q_g D\rho(dm/dT) \quad , \tag{8}$$

where the first term on the right hand side is the frozen component, i.e., the true thermal conductivity, and the second term the reactive component. This equation can be generalized to the case of a arbitrary number of species related by a full set of reactions. There the dm/dT term is replaced by a sum over the dm_i/dT for each species i. If the system is in chemical equilibrium, one can compute the reactive component and treat the system as a non-reactive one with known effective conductivity. Thus the heat flow problem can be greatly simplified where convection is not involved and chemical equilibrium applies. Since convection is an important process in propellant burning, the reactive component computed in Reference 23 is not relevant to our purpose, though the frozen component is, provided the thermal equilibrium assumption is not too restrictive.

While the chemical equilibrium assumption obviously is not valid through the secondary flame zone, it should be reasonable at the high temperature end of the zone. Presumably, the non-equilibrium composition of Table 2 is appropriate at the low temperature end of the zone. Using Fifer and Cohen's frozen transport values[23] at 0.95 atm and 2957 K for the double base propellant, M9, and our best estimate values at 1600 K, we expect a reasonable estimate of the transport parameters in the secondary flame to be given by

$$\lambda = 1.49 \times 10^{-8} T^{0.750} \quad \text{cal/cm-s-K} \tag{9}$$

$$c_p = 0.767 T^{-0.0763} \quad \text{cal/g-K} \tag{10}$$

for T in Kelvins. Though the negative exponent for the specific heat is not typical of pure gases, in principle it should be possible for shifts in composition. In any event the indicated decrease with temperature is slight.

VII. CONCLUSIONS

This study was undertaken in order to assess the importance of having accurate values for the thermal conductivity and specific heat for the gas mixture in the primary flame zone of double base propellants. These transport variables are required in order to derive effective kinetics for the heat release in that zone. Such an assessment was considered to be a prerequisite to a determination of the feasibility and desirability of measuring the major species in the primary flame by means of mass spectrometry.

Using published species concentrations measured for a double base propellant, mixture properties both at the burning surface and at the end of the primary flame zone were computed and varied by assuming concentrations of

the critical species to be in error by a factor of 2. Relative to a best estimate value this error results in an error of less than 25% for the thermal conductivity and less than 30% for the specific heat. The relative insensitivity of the transport properties to the species concentrations can be understood by the following reasoning. The thermal conductivity is roughly proportional to the product of the mean molecular velocity and the molar specific heat. In general, the larger molecules have higher molar specific heats and lower velocities at the same temperature. Thus, these two factors at least partially compensate for each other as a function of molecule size. The mass specific heat, being the ratio of the molar specific heat and the molecular weight also tends to vary only slightly with increasing molecule size.

The guiding concern in this paper has been the extent to which the probable uncertainty in λ and c_p might affect the accuracy of model descriptions of propellant combustion. The sensitivity of model parameters, derived by a semi-empirical method, to these uncertainties was therefore first determined. The largest error, about 85%, was in the condensed phase heat release Q_s, which should have the greatest effect on the temperature sensitivity of the burning rate. The fizz zone heat release and activation energy could be in error by up to 25%.

Next a calculation of the burning rate using these parameters was performed. It was found that the burning rate computed at the calibration temperature was in error, due to uncertain transport values, by less than 2%. The heat feedback to the burning surface could be inaccurate by up to 30%, a finding that may have significant consequences for use of the model in transient combustion. Due to the large effect of possible transport errors on the condensed phase heat release, calculations of the burning rate at ambient temperatures spanning the range of practical interest were performed. Errors of up to 7% were noted.

The conclusion of this study is, thus, fairly clear. Probable uncertainties in the transport properties of the fizz zone, arising from uncertainties in the major species there, do not have a significant effect on our ability to do accurate model calculations of the steady-state burning rate. These uncertainties do, however, lead to substantial differences in the derived values of the condensed phase heat release, which may be important for a proper treatment of transient combustion, where accurate descriptions for the phenomena in each phase is more important. While such calculations would be a worthwhile future task, our judgement at this time is that transport uncertainties are not the limiting factor in the semi-empirical modeling strategy presently under development, and therefore is not in itself a strong justification for doing the molecular beam sampling experiment.

REFERENCES

1. T.P. Coffee, A.J. Kotlar, and M.S. Miller, "The Overall Reaction Concept in Premixed, Laminar, Steady-State Flames. I. Stoichiometries," Combustion & Flame, Vol. 54, pp. 155-169, 1983.

2. T.P. Coffee, A.J. Kotlar, and M.S. Miller, "The Overall Reaction Concept in Premixed, Laminar, Steady-State Flames. II. Pressure and Initial Temperature," Combustion & Flame, Vol. 58, pp. 59-67, 1984.

3. T.P. Coffee, A.J. Kotlar, and M.S. Miller, "Applicability of the Overall Reaction Concept to Propellant Combustion," Proceedings of the 21st JANNAF Combustion Meeting, October 1984.

4. A.J. Kotlar, M.S. Miller, and T.P. Coffee, "Effective Kinetic Parameters for Gas Phase Heat Release During Solid Propellant Combustion," Proceedings of the 21st JANNAF Combustion Meeting, October 1984.

5. G. Lengelle, A. Bizot, J. Duterque, and J.F. Trubert, "Steady-State Burning of Homogeneous Propellants", in "Fundamentals of Solid-Propellant Combustion", edited by Kenneth K. Kuo and Martin Summerfield, Vol. 90, in Progress in Astronautics and Aeronautics series, American Institute of Aeronautics and Astronautics, Inc., 1984.

6. G. Lengelle, J. Duterque, C. Verdier, A. Bizot, and J.F. Trubert, "Combustion Mechanisms of Double-Base Solid Propellants," 17th Symposium (International) on Combustion, The Combustion Institute, Pittsburgh, PA, pp. 1443-1451, 1979.

7. L. Dauerman, G.E. Salser, and Y.A. Tajima, "Characterization of Volatilized Species from Solid Propellants," AIAA Journal, Vol. 5, pp. 1501-1503, 1967.

8. L. Dauerman and Y.A. Tajima, "Solid-Phase Reactions of a Double-Base Propellant," AIAA Journal, Vol. 6, pp. 678-683, 1968.

9. L. Dauerman and Y.A. Tajima, "Thermal Decomposition and Combustion of Nitrocellulose," AIAA Journal, Vol. 6, pp. 1468-1473, 1968.

10. M. Farber and R.D. Srivastava, "A Mass-Spectrometric Investigation of the Chemistry of Plateau Burning Propellants," Combustion and Flame, Vol. 31, pp. 309-323, 1978.

11. C.A. Heller and A.S. Gordon, "Structure of the Gas Phase Combustion Region of a Solid Double Base Propellant," J. of Physical and Colloid Chemistry, Vol. 59, pp. 773-777, 1955.

12. Y.S. Touloukian, P.E. Liley, and S.C. Saxena, Thermal Conductivity - Nonmetallic Liquids and Gases, IFI/Plenum Data Corp., New York, 1970.

13. R.A. Svehla and B.J. McBride, "Fortran IV Computer Program for Calculation of Thermodynamic and Transport Properties of Complex Chemical Systems," NASA Technical Note D-7056, Lewis Research Center, Cleveland, OH, January 1973.

14. R.C. Reid, J.M. Prausnitz, and T.K. Sherwood, The Properties of Gases and Liquids, 3rd Edition, McGraw-Hill, New York, 1977.

15. J.H. Burgoyne and F. Weinberg, "A Method of Analysis of a Plane Combustion Wave," Fourth Symposium on Combustion (International), Williams and Wilkins Co., Baltimore, pp. 294-302, 1953.

16. L.I. Stiel and G. Thodos, "The Thermal Conductivity of Nonpolar Substances in the Dense Gaseous and Liquid Regions," AIChE J., Vol. 10, pp. 26-30, 1964.

17. D.R. Stull and H. Prophet, JANAF Thermochemical Tables, 2nd Ed., NSRDS-NBS-37, June 1957.

18. A.A. Zenin, "Structure of Temperature Distribution in Steady-State Burning of a Ballistite Powder", Fizika Goreniya i Vzryva, Vol. 2, pp. 67-76, 1966.

19. M.S. Miller, "In Search of an Idealized Model of Homogeneous Solid Propellant Combustion", Comb. and Flame, Vol. 46, pp. 51-73, 1982.

20. M.S. Miller and T.P. Coffee, "A Fresh Look at the Classical Approach to Homogeneous Solid Propellant Combustion Modeling", Comb. and Flame, Vol. 50, pp. 65-74, 1983.

21. M.S. Miller and T.P. Coffee, "On the Numerical Accuracy of Homogeneous Solid Propellant Combustion Models", Comb. and Flame, Vol. 50, pp. 75-88, 1983.

22. M.S. Miller, T.P. Coffee, A.J. Kotlar, "Imbedded Thermocouples as a Solid Propellant Combustion Probe", BRL Memorandum Report BRL-MR-3440 (AD155630), April 1985.

23. R.A. Fifer and A. Cohen, "High Temperature Thermal Conductivity and Heat Transfer in Gun Propellant and Primer Combustion Gases", 14th JANNAF Combustion Meeting, CPIA Publication 292, Vol. II, pp. 363-387, 1977.

A-1 G. Arfken, Mathematical Methods for Physicists, 2nd Ed., Academic Press, New York, p. 419, 1973.

APPENDIX: TEMPERATURE PROFILE FITTING FUNCTION

APPENDIX TEMPERATURE PROFILE FITTING FUNCTION

The choice of the functional representation of the temperature is based on the generally observed sigmoidal shape of the experimental distributions. The rationale for the chosen function is outlined here.

The function

$$S_n = [1 + \tanh(nx)]$$

which in the limit of large n becomes the Heavyside step function,[A-1] provides the basic features of the required shape. A number of parameters, designated p_1 through p_9, are included to give the function greater flexibility and proper scale. Parameters p_1 and p_2 adjust the plateau regions of the function to the correct initial and final temperature asymptotes, p_3 repositions the function along the x axis, p_4 through p_8 form a polynomial expansion for the argument of tanh, which allows for asymmetry in the function, which is then raised to a power, (p_9+1). Summarizing these considerations:

$$f(x) = (p_2-p_1)h(u) + p_1 \tag{A1}$$

where

$$h(u) = [(1 + \tanh u)/2]^{(p_9+1)} ,$$
$$u = p_4 z + p_5 z^2 + p_6 z^3 + p_7 z^4 + p_8 z^5 , \tag{A2}$$

and

$$z = x - p_3 . \tag{A3}$$

In general this function has sufficient flexibility to simulate the experimental temperature profile. Occasionally, however, there is one particular region where the function does not adequately reproduce the data. An additional expression, having the form of a skewed Gaussian function, which may be sharply peaked in one area, is therefore included. This expression is normalized for greater numerical stability, and is described by parameters p_{10} through p_{13} as follows:

$$g(v) = 1 + G(v)/G_N , \tag{A4}$$

where

$$G(v) = p_{11} \exp(-a^2 v^2 + p_{13} v) , \tag{A5}$$

$$a^2 = 4 \ln 2/p_{12}^2 , \tag{A6}$$

$$v = x - p_{10} , \tag{A7}$$

$$G_N = \exp(-a^2 v_N + p_{13} v_N) , \tag{A8}$$

and

$$v_N = p_{13}/2a^2 \quad . \tag{A9}$$

For $p_{13} = 0$, p_{12} is the full width at half maximum of a Gaussian function centered at p_{10}.

The full representation of the temperature function is then

$$T(x) = (p_2-p_1)\ h(u)\ g(v) + p_1 \tag{A10}$$

where h(u) is given by Eqs. (A1)-(A3) and g(v) is given by Eqs. (A4)-(A9).

DISTRIBUTION LIST

No. Of Copies	Organization
12	Administrator Defense Technical Info Center ATTN: DTIC-DDA Cameron Station Alexandria, VA 22304-6145
1	HQ DA DAMA-ART-M Washington, DC 20310
1	Commander US Army Materiel Command ATTN: AMCDRA-ST 5001 Eisenhower Avenue Alexandria, VA 22333-0001
10	Central Intelligence Agency Office of Central Reference Dissemination Branch Room GE-47 HQS Washington, DC 20505
1	Commander Armament R&D Center US Army AMCCOM ATTN: SMCAR-TSS Dover, NJ 07801
1	Commander Armament R&D Center US Army AMCCOM ATTN: SMCAR-TDC Dover, NJ 07801
1	Director Benet Weapons Laboratory Armament R&D Center US Army AMCCOM ATTN: SMCAR-LCB-TL Watervliet, NY 12189
1	Commander US Army Armament, Munitions and Chemical Command ATTN: SMCAR-ESP-L Rock Island, IL 61299
1	Commander US Army Aviation Research and Development Command ATTN: AMSAV-E 4300 Goodfellow Blvd. St. Louis, MO 63120
1	Director US Army Air Mobility Research and Development Laboratory Ames Research Center Moffett Field, CA 94035
4	Commander US Army Research Office ATTN: R. Ghirardelli D. Mann R. Singleton R. Shaw P.O. Box 12211 Research Triangle Park, NC 27709-2211
1	Commander US Army Communications - Electronics Command ATTN: AMSEL-ED Fort Monmouth, NJ 07703
1	Commander, U.S. Army Communications - Electronics Command (CECOM) CECOM R&D Technical Library ATTN: AMSEL-IM-L B 2700 Fort Monmouth, NJ 07703-5000
2	Commander Armament R&D Center US Army AMCCOM ATTN: SMCAR-LCA-G, D.S. Downs J.A. Lannon Dover, NJ 07801
1	Commander Armament R&D Center US Army AMCCOM ATTN: SMCAR-LC-G, L. Harris Dover, NJ 07801

DISTRIBUTION LIST

No. Of Copies	Organization
1	Commander Armament R&D Center US Army AMCCOM ATTN: SMCAR-SCA-T, L. Stiefel Dover, NJ 07801
1	Commander US Army Missile Command Research, Development and Engineering Center ATTN: AMSMI-RD Redstone Arsenal, AL 35898
1	Commander US Army Missile and Space Intelligence Center ATTN: AMSMI-YDL Redstone Arsenal, AL 35898-5000
2	Commander US Army Missile Command ATTN: AMSMI-RK, D.J. Ifshin W. Wharton Redstone Arsenal, AL 35898
1	Commander US Army Missile Command ATTN: AMSMI-RKA, A.R. Maykut Redstone Arsenal, AL 35898-5249
1	Commander US Army Tank Automotive Command ATTN: AMSTA-TSL Warren, MI 48397-5000
1	Director US Army TRADOC Systems Analysis Activity ATTN: ATAA-SL White Sands Missile Range, NM 88002
1	Commandant US Army Infantry School ATTN: ATSH-CD-CSO-OR Fort Benning, GA 31905
1	Commander US Army Development and Employment Agency ATTN: MODE-TED-SAB Fort Lewis, WA 98433
1	Office of Naval Research Department of the Navy ATTN: R.S. Miller, Code 432 800 N. Quincy Street Arlington, VA 22217
1	Commander Naval Air Systems Command ATTN: J. Ramnarace, AIR-54111C Washington, DC 20360
2	Commander Naval Ordnance Station ATTN: C. Irish P.L. Stang, Code 515 Indian Head, MD 20640
1	Commander Naval Surface Weapons Center ATTN: J.L. East, Jr., G-23 Dahlgren, VA 22448-5000
2	Commander Naval Surface Weapons Center ATTN: R. Bernecker, R-13 G.B. Wilmot, R-16 Silver Spring, MD 20902-5000
1	Commander Naval Weapons Center ATTN: R.L. Derr, Code 389 China Lake, CA 93555
2	Commander Naval Weapons Center ATTN: Code 3891, T. Boggs K.J. Graham China Lake, CA 93555

DISTRIBUTION LIST

No. Of Copies	Organization
5	Commander Naval Research Laboratory ATTN: M.C. Lin J. McDonald E. Oran J. Shnur R.J. Doyle, Code 6110 Washington, DC 20375
1	Commanding Officer Naval Underwater Systems Center Weapons Dept. ATTN: R.S. Lazar/Code 36301 Newport, RI 02840
1	Superintendent Naval Postgraduate School Dept. of Aeronautics ATTN: D.W. Netzer Monterey, CA 93940
4	AFRPL/DY, Stop 24 ATTN: R. Corley R. Geisler J. Levine D. Weaver Edwards AFB, CA 93523-5000
1	AFRPL/MKPB, Stop 24 ATTN: B. Goshgarian Edwards AFB, CA 93523-5000
1	AFOSR ATTN: J.M. Tishkoff Bolling Air Force Base Washington, DC 20332
1	Air Force Armament Laboratory ATTN: AFATL/DLODL Eglin AFB, FL 32542-5000
1	Air Force Weapons Laboratory AFWL/SUL ATTN: V. King Kirtland AFB, NM 87117
1	NASA Langley Research Center Langley Station ATTN: G.B. Northam/MS 168 Hampton, VA 23365
4	National Bureau of Standards ATTN: J. Hastie M. Jacox T. Kashiwagi H. Semerjian US Department of Commerce Washington, DC 20234
1	OSD/SDIO/UST ATTN: L.H. Caveny Pentagon Washington, DC 20301-7100
1	Aerojet Solid Propulsion Co. ATTN: P. Micheli Sacramento, CA 95813
1	Applied Combustion Technology, Inc. ATTN: A.M. Varney P.O. Box 17885 Orlando, FL 32860
2	Applied Mechanics Reviews The American Society of Mechanical Engineers ATTN: R.E. White A.B. Wenzel 345 E. 47th Street New York, NY 10017
1	Atlantic Research Corp. ATTN: M.K. King 5390 Cherokee Avenue Alexandria, VA 22314
1	Atlantic Research Corp. ATTN: R.H.W. Waesche 7511 Wellington Road Gainesville, VA 22065

DISTRIBUTION LIST

No. Of Copies	Organization
1	AVCO Everett Rsch. Lab. Div. ATTN: D. Stickler 2385 Revere Beach Parkway Everett, MA 02149
1	Battelle Memorial Institute Tactical Technology Center ATTN: J. Huggins 505 King Avenue Columbus, OH 43201
1	Cohen Professional Services ATTN: N.S. Cohen 141 Channing Street Redlands, CA 92373
1	Exxon Research & Eng. Co. Government Research Lab ATTN: A. Dean P.O. Box 48 Linden, NJ 07036
1	Ford Aerospace and Communications Corp. DIVAD Division Div. Hq., Irvine ATTN: D. Williams Main Street & Ford Road Newport Beach, CA 92663
1	General Applied Science Laboratories, Inc. ATTN: J.I. Erdos 425 Merrick Avenue Westbury, NY 11590
1	General Electric Armament & Electrical Systems ATTN: M.J. Bulman Lakeside Avenue Burlington, VT 05401
1	General Electric Company 2352 Jade Lane Schenectady, NY 12309
1	General Electric Ordnance Systems ATTN: J. Mandzy 100 Plastics Avenue Pittsfield, MA 01203
2	General Motors Rsch Labs Physics Department ATTN: T. Sloan R. Teets Warren, MI 48090
2	Hercules, Inc. Allegany Ballistics Lab. ATTN: R.R. Miller E.A. Yount P.O. Box 210 Cumberland, MD 21501
1	Hercules, Inc. Bacchus Works ATTN: K.P. McCarty P.O. Box 98 Magna, UT 84044
1	Honeywell, Inc. Government and Aerospace Products ATTN: D.E. Broden/ MS MN50-2000 600 2nd Street NE Hopkins, MN 55343
1	IBM Corporation ATTN: A.C. Tam Research Division 5600 Cottle Road San Jose, CA 95193
1	IIT Research Institute ATTN: R.F. Remaly 10 West 35th Street Chicago, IL 60616

DISTRIBUTION LIST

No. Of Copies	Organization
2	Director Lawrence Livermore National Laboratory ATTN: C. Westbrook M. Costantino P.O. Box 808 Livermore, CA 94550
1	Lockheed Missiles & Space Co. ATTN: George Lo 3251 Hanover Street Dept. 52-35/B204/2 Palo Alto, CA 94304
1	Los Alamos National Lab ATTN: B. Nichols T7, MS-B284 P.O. Box 1663 Los Alamos, NM 87545
1	National Science Foundation ATTN: A.B. Harvey Washington, DC 20550
1	Olin Corporation Smokeless Powder Operations ATTN: V. McDonald P.O. Box 222 St. Marks, FL 32355
1	Paul Gough Associates, Inc. ATTN: P.S. Gough 1048 South Street Portsmouth, NH 03801
2	Princeton Combustion Research Laboratories, Inc. ATTN: M. Summerfield N.A. Messina 475 US Highway One Monmouth Junction, NJ 08852
1	Hughes Aircraft Company ATTN: T.E. Ward 8433 Fallbrook Avenue Canoga Park, CA 91303
1	Rockwell International Corp. Rocketdyne Division ATTN: J.E. Flanagan/HB02 6633 Canoga Avenue Canoga Park, CA 91304
4	Sandia National Laboratories Combustion Sciences Dept. ATTN: R. Cattolica S. Johnston P. Mattern D. Stephenson Livermore, CA 94550
1	Science Applications, Inc. ATTN: R.B. Edelman 23146 Cumorah Crest Woodland Hills, CA 91364
1	Science Applications, Inc. ATTN: H.S. Pergament 1100 State Road, Bldg. N Princeton, NJ 08540
3	SRI International ATTN: G. Smith D. Crosley D. Golden 333 Ravenswood Avenue Menlo Park, CA 94025
1	Stevens Institute of Tech. Davidson Laboratory ATTN: R. McAlevy, III Hoboken, NJ 07030
1	Textron, Inc. Bell Aerospace Co. Division ATTN: T.M. Ferger P.O. Box 1 Buffalo, NY 14240
1	Thiokol Corporation Elkton Division ATTN: W.N. Brundige P.O. Box 241 Elkton, MD 21921

DISTRIBUTION LIST

No. Of Copies	Organization
1	Thiokol Corporation Huntsville Division ATTN: R. Glick Huntsville, AL 35807
3	Thiokol Corporation Wasatch Division ATTN: S.J. Bennett P.O. Box 524 Brigham City, UT 84302
1	TRW ATTN: M.S. Chou MSR1-1016 1 Parke Redondo Beach, CA 90278
1	United Technologies ATTN: A.C. Eckbreth East Hartford, CT 06108
3	United Technologies Corp. Chemical Systems Division ATTN: R.S. Brown T.D. Myers (2 copies) P.O. Box 50015 San Jose, CA 95150-0015
2	United Technologies Corp. ATTN: R.S. Brown R.O. McLaren P.O. Box 358 Sunnyvale, CA 94086
1	Universal Propulsion Company ATTN: H.J. McSpadden Black Canyon Stage 1 Box 1140 Phoenix, AZ 85029
1	Veritay Technology, Inc. ATTN: E.B. Fisher 4845 Millersport Highway P.O. Box 305 East Amherst, NY 14051-0305
1	Brigham Young University Dept. of Chemical Engineering ATTN: M.W. Beckstead Provo, UT 84601
1	California Institute of Tech. Jet Propulsion Laboratory ATTN: MS 125/159 4800 Oak Grove Drive Pasadena, CA 91103
1	California Institute of Technology ATTN: F.E.C. Culick/ MC 301-46 204 Karman Lab. Pasadena, CA 91125
1	University of California, Berkeley Mechanical Engineering Dept. ATTN: J. Daily Berkeley, CA 94720
1	University of California Los Alamos Scientific Lab. P.O. Box 1663, Mail Stop B216 Los Alamos, NM 87545
2	University of California, Santa Barbara Quantum Institute ATTN: K. Schofield M. Steinberg Santa Barbara, CA 93106
2	University of Southern California Dept. of Chemistry ATTN: S. Benson C. Wittig Los Angeles, CA 90007
1	Case Western Reserve Univ. Div. of Aerospace Sciences ATTN: J. Tien Cleveland, OH 44135

DISTRIBUTION LIST

No. Of Copies	Organization
1	Cornell University Department of Chemistry ATTN: T.A. Cool Baker Laboratory Ithaca, NY 14853
1	Univ. of Dayton Rsch Inst. ATTN: D. Campbell AFRPL/PAP Stop 24 Edwards AFB, CA 93523
1	University of Florida Dept. of Chemistry ATTN: J. Winefordner Gainesville, FL 32611
3	Georgia Institute of Technology School of Aerospace Engineering ATTN: E. Price W.C. Strahle B.T. Zinn Atlanta, GA 30332
1	University of Illinois Dept. of Mech. Eng. ATTN: H. Krier 144MEB, 1206 W. Green St. Urbana, IL 61801
1	Johns Hopkins University/APL Chemical Propulsion Information Agency ATTN: T.W. Christian Johns Hopkins Road Laurel, MD 20707
1	University of Michigan Gas Dynamics Lab Aerospace Engineering Bldg. ATTN: G.M. Faeth Ann Arbor, MI 48109-2140
1	University of Minnesota Dept. of Mechanical Engineering ATTN: E. Fletcher Minneapolis, MN 55455
3	Pennsylvania State University Applied Research Laboratory ATTN: K.K. Kuo H. Palmer M. Micci University Park, PA 16802
1	Polytechnic Institute of NY Graduate Center ATTN: S. Lederman Route 110 Farmingdale, NY 11735
2	Princeton University Forrestal Campus Library ATTN: K. Brezinsky I. Glassman P.O. Box 710 Princeton, NJ 08540
1	Princeton University MAE Dept. ATTN: F.A. Williams Princeton, NJ 08544
1	Purdue University School of Aeronautics and Astronautics ATTN: J.R. Osborn Grissom Hall West Lafayette, IN 47906
1	Purdue University Department of Chemistry ATTN: E. Grant West Lafayette, IN 47906
2	Purdue University School of Mechanical Engineering ATTN: N.M. Laurendeau S.N.B. Murthy TSPC Chaffee Hall West Lafayette, IN 47906
1	Rensselaer Polytechnic Inst. Dept. of Chemical Engineering ATTN: A. Fontijn Troy, NY 12181

DISTRIBUTION LIST

No. Of Copies	Organization
1	Stanford University Dept. of Mechanical Engineering ATTN: R. Hanson Stanford, CA 94305
1	University of Texas Dept. of Chemistry ATTN: W. Gardiner Austin, TX 78712
1	University of Utah Dept. of Chemical Engineering ATTN: G. Flandro Salt Lake City, UT 84112
1	Virginia Polytechnic Institute and State University ATTN: J.A. Schetz Blacksburg, VA 24061
1	Commandant USAFAS ATTN: ATSF-TSM-CN Fort Sill, OK 73503-5600

Aberdeen Proving Ground

Dir, USAMSAA
ATTN: AMXSY-D
AMXSY-MP, H. Cohen
Cdr, USATECOM
ATTN: AMSTE-TO-F
Cdr, CRDC, AMCCOM
ATTN: SMCCR-RSP-A
SMCCR-MU
SMCCR-SPS-IL

USER EVALUATION SHEET/CHANGE OF ADDRESS

This Laboratory undertakes a continuing effort to improve the quality of the reports it publishes. Your comments/answers to the items/questions below will aid us in our efforts.

1. BRL Report Number _____ Date of Report _____

2. Date Report Received _____

3. Does this report satisfy a need? (Comment on purpose, related project, or other area of interest for which the report will be used.) _____

_____

_____

4. How specifically, is the report being used? (Information source, design data, procedure, source of ideas, etc.) _____

_____

_____

5. Has the information in this report led to any quantitative savings as far as man-hours or dollars saved, operating costs avoided or efficiencies achieved, etc? If so, please elaborate. _____

_____

_____

6. General Comments. What do you think should be changed to improve future reports? (Indicate changes to organization, technical content, format, etc.)

_____

_____

_____

CURRENT ADDRESS

_____
Name

_____
Organization

_____
Address

_____
City, State, Zip

7. If indicating a Change of Address or Address Correction, please provide the New or Correct Address in Block 6 above and the Old or Incorrect address below.

OLD ADDRESS

_____
Name

_____
Organization

_____
Address

_____
City, State, Zip

(Remove this sheet along the perforation, fold as indicated, staple or tape closed, and mail.)

FOLD HERE

Director
U.S. Army Ballistic Research Laboratory
ATTN: SLCBR-DD-T
Aberdeen Proving Ground, MD 21005-5066

NO POSTAGE
NECESSARY
IF MAILED
IN THE
UNITED STATES

OFFICIAL BUSINESS
PENALTY FOR PRIVATE USE, $300

BUSINESS REPLY MAIL
FIRST CLASS PERMIT NO 12062 WASHINGTON, DC
POSTAGE WILL BE PAID BY DEPARTMENT OF THE ARMY

Director
U.S. Army Ballistic Research Laboratory
ATTN: SLCBR-DD-T
Aberdeen Proving Ground, MD 21005-9989

FOLD HERE

END

4-87

DTIC